Astron. Astrophys. 353, 823–833 (2000)

ASTRONOMY AND ASTROPHYSICS

On the matter distribution of galaxy clusters containing a compact core

Tzihong Chiueh[1,3] **and Xiang-Ping Wu**[2]

[1] Department of Physics, National Taiwan University, Taipei, Taiwan, R.O.C.
[2] Beijing Astronomical Observatory and National Astronomical Observatories, Chinese Academy of Sciences, Beijing, P.R. China
[3] Institute of Astronomy and Astrophysics, Academia Sinica, Taipei, Taiwan, R.O.C.

Received 23 June 1999 / Accepted 19 November 1999

Abstract. Increasing evidences provided primarily by the cluster lensing and numerical simulations of cluster formation indicate that galaxy clusters may contain compact cores that are substantially smaller than the cores revealed by the X-ray observations of hot intracluster gas. In this paper we present a model that describes how two distinct cores can grow simultaneously as a result of infall from the background dark matter. This model needs a pre-existing localized large fluctuation, which can be the non-Gaussian density peak of the primordial fluctuations, to seed the individual growing cluster. On the other hand, numerous recent observations also show that no strong evolution is detected for galaxy clusters within the redshift up to $z \sim 0.8$. We therefore present a comparison of observations with the saturated cluster configuration resulting from our infall model. In the saturated state, the predicted compact core mass is about few$\times 10^{11} M_\odot$ and the core size about 1 kpc for a cluster mass $\sim$ several $\times 10^{15} M_\odot$ within a radius of 3 Mpc. We have successfully reproduced the dark matter distribution revealed by the gravitational lensing, and the observed radial distributions of cluster galaxies, intracluster gas (i.e., the conventional β model) and baryon fractions in a consistent way. This model, when combined with the observed X-ray surface brightness profiles of clusters, predicts that the overall temperature of intracluster gas has a tendency of radial decline with a mean polytropic index $\gamma \approx 1.2$. Finally, the so-called β discrepancy finds a natural explanation for such a polytropic gas in our model.

Key words: hydrodynamics – galaxies: clusters: general – cosmology: theory – cosmology: dark matter

1. Introduction

The existence of a compact and massive dark-matter core in the galaxy cluster, which is much smaller than the X-ray gas core of the empirical β model, has recently acquired substantial supports from various evidences. It has been recognized since the early study of the very thin arclike images of distant galaxies created by the potentials of the foreground lensing clusters that the dark matter profiles of the lensing clusters should be sharply peaked towards cluster centers (e.g. Hammer 1991). In order to account for the total number of observed giant luminous arcs, the core size of dark matter distribution modeled by a softened isothermal sphere should be at least ~ 10 times smaller than the one for luminous matter profile (Wu & Hammer 1993). Grossman & Saha (1994) strengthened this argument by explicitly setting an unprecedentedly small upper limit on cluster core radius, $r_{dark,c} < 11$ kpc, for a softened isothermal sphere. Many recent work on modeling of arcs/arclets have essentially confirmed these findings (e.g. Giraud 1999; William, Navarro & Bartelmann 1999). Even for the X-ray measurements of hot intracluster gas, the dynamical analysis also arrives at a similar conclusion that the binding matter distribution of clusters should have a core radius of $r_{dark,c} < 100$ kpc (Durret et al. 1994). Optically, the omni-presence of cD galaxies in the cores of many rich clusters may indicate unusual accumulation of central masses. Finally, a singular mass profile of $\rho \propto r^{-1}$ at cluster center is predicted by the numerical studies of cluster formation in the framework of the standard CDM model as well as other cosmological models (e.g. Navarro et al. 1995; Cole & Lacey 1996; Navarro, Frenk & White 1997; Fukushige & Makino 1997; Eke, Navarro & Frenk 1998). Such a singular mass profile also houses a weak compact core.

That is, while the cluster X-ray gas often shows a core of typical size about $100-250$ kpc, the dark matter core can instead be substantially smaller than 100 kpc. The co-existence of two distinct mass cores in a single cluster appears to have challenged our current understanding of cluster formation. Although a great deal of theoretical efforts have in the past been put forth attempting to grasp an understanding of the cluster physics, few have considered the possibility of a massive compact dark matter core in the galaxy cluster. Past analytic investigations for the gravitational infall of matter into galaxy clusters have been pursued mainly toward the following two issues: the cosmic evolution of cluster properties such as the total mass, number counts, gas luminosity and temperature (e.g. Gunn & Gott 1972; Press & Schechter 1974; Kaiser 1986; 1991), as well as the gas and dark matter density profiles inside clusters (e.g. Fillmore & Goldre-

Send offprint requests to: T. Chiueh
Correspondence to: chiuehth@phys.ntu.edu.tw

ich 1984; Bertschinger 1985; Teyssier, Chièze & Alimi 1997). Regardless of their oversimplification, these analytic treatments based on self-similar models indeed provide the gross properties of clusters that were shown to be in gross consistency with optical/X-ray observations (Kaiser 1991). Moreover, these analytical studies can also reveal the underlying cluster evolution mechanisms, in a complementary manner to those shown by the particle and hydrodynamic simulations. In spite of the past success, previous studies commonly obtained (or assumed) a single core within the cluster.

In the self-similar regime, clusters are, however, shown to undergo very rapid evolution (Gunn & Gott 1972; Kaiser 1986). When these results are combined with the recent observations made primarily at X-ray wavebands, which demonstrate that no evolution has been detected within the redshift at least out to $z \approx 0.8$ among the cluster number counts, X-ray luminosity, temperature function as well as typical scale lengths (e.g. Fan, Bahcall & Cen 1997; Rosati et al. 1998; Vikhlinin et al. 1998; Wu, Xue & Fang 1999 and references therein), one is led to a conclusion that the evolution of these clusters must have ended at an early epoch.

In this paper, we will concentrate on the dark matter and the galaxy/gas distributions of clusters revealed mainly by the saturated state of a new class of self-similar infall model, which describes the simultaneous build-up of two distinct cores in a single cluster. Our starting point differs from the past theoretical models in the following way: (a) Unlike the previous work which chose a power-law initial perturbation in the mass (e.g. Fillmore & Goldreich 1984; Teyssier et al. 1997), we seek a solution to the infall problem of dark matter particles by assuming an initial compact seed density fluctuation at the site of growing cluster. This aspect is in line with the works of Gott (1975) and Bertschinger (1985), and the large-amplitude seed fluctuation may arise from a non-Gaussian peak in the primordial density fluctuations. (b) Instead of assuming the collisionless particles to move with radial orbits (Merritt, Tremaine & Johnstone 1989), which are known to be unstable (Binney & Tremaine 1987), we consider the other extreme situation where the particle orbits inside the cluster are so chaotic that the velocity dispersion is essentially isotropic.

After a substantial growth of both cores, they can rapidly reach a saturated state, in which the mass ratio of the two cores remains approximately the same as that during the infall phase. (This is because both cores are gravitationally bound, and they have been grossly virialized regardless of whether there exists an infall.) Our attempt at comparing the theoretical predictions with observational results will therefore be made at this late stage when the matter infall has ended, and a hydrostatic equilibrium has already been established between the dark-matter gravitational potential and the cluster galaxies and intracluster gas.

We begin in Sect. 2 by presenting a specific model describing the self-similar evolution of spherical collapse of collisionless cold dark matter in an open and a closed universe. (The former also represents the situation where the infall began only recently and is still ongoing in a flat universe.) We then derive the density profiles of dark matter in the infall phase and in the saturated phase, respectively. In Sect. 3 the predicted dark matter distribution and the galaxy/gas density profiles are compared with those revealed by the gravitational lensing and optical/X-ray observations. Finally, the discussion and summary are given in Sect. 4. Beginning from Sect. 3, where comparisons of the theoretical predictions with the observations are made, we work mainly with the saturated state (except in Sect. 3.1), and the Hubble constant is chosen to be $H_0 = 50$ km s^{-1} Mpc^{-1} for convenience. Throughout this work, we set the cosmological constant equal to zero.

2. Self-similar solutions for the collapse of cold dark matter

2.1. Physical picture and mathematical formulation

Assuming the linear growth of an overdense spherical top-hat perturbation, Gott (1975) and Bertschinger (1985) have derived that a bound object can grow, as a result of matter infall from the pressureless Hubble flow, with the time dependence: $M \propto t^{2/3}$ and $r_m \propto t^{8/9}$, where M is the total mass within the radius r_m of the growing bound object and t is the evolution time. Such a scaling relation depends only weakly on the decelerating parameter q_0 (for $0.02 < q_0 < 2$), and these relations become exact when $q_0 = 1/2$. A slightly different scaling relation has also been predicted by Press and Schechter (1974) in their quest for the galaxy mass function. They found that $M \propto t^{4/3}$ and $r_m \propto t^{10/9}$. A feature common to both scaling relations is that the characteristic length scale r_m is approximately a linear function of time. This behavior will be used to fix the temporal scaling of velocity as t^0 in our self-similar model.

On the other hand, the crossing of mass shells near the core can trigger particle orbit instabilities that yield violent relaxation (Lynden-Bell 1967). The particle orbits may be further randomized by the interactions with the crowded discrete galaxies in the cluster, making the dark matter particles further mixed. We therefore approximate the dark matter within the cluster to have an isotropic and also spatially uniform velocity dispersion σ_d. Together with the temporal scaling discussed in the last paragraph, one may consider σ_d to be a constant in space and in time within the cluster. (For readers who have a different view of how the dark matter particles should behave in the cluster, they may simply regard the constant σ_d as a working hypothesis adopted to fix the self-similar scaling relations.) Outside the cluster, the cold dark matter detached from the expanding background Hubble flow falls radially inwards. The boundary of the hot cluster and cold background is defined by a heat conduction front, across which both mass flux and momentum flux are continuous.

Thus, our picture of the self-similar matter infall can be summarized as follows. As the cold dark matter falls towards the massive compact core, a volume of finite radius surrounding the compact core then undergoes violent relaxation and forms an isothermal halo, which gives rise to the cluster potential. A small fraction of the infall particles can however sink into the compact core and therefore the peak of the central density can grow steadily (Gott 1975). But the majority of infall particles

are deflected back to the halo. The deflected particles find the halo to become more massive than they previously experienced due to the continuing infall, and hence the particles can travel only up to a maximum radius, which defines the location of the conduction front, i.e., the boundary of the hot cluster. As these processes continue, both compact core and halo can grow self-consistently.

To put this picture into a quantitative perspective, we adopt a spherically symmetric infall model. Since the particle orbits are assumed to be isotropic in the cluster bulk, the anisotropic stress force is unimportant and it suffices to consider only the radial pressure force in the momentum balance. The unique self-similar scaling with a constant σ_d requires the mass density of dark matter particles $\rho(r,t)$, the flow speed $u(r,t)$ and the total mass $M(r,t)$ enclosed within radius r to be scaled as:

$$\rho(r,t)=\frac{\alpha(x)}{4\pi G\tau^2},\quad u(r,t)=\sigma_d v(x),\quad M(r,t)=\frac{\sigma_d^3\tau}{G}m(x), \tag{1}$$

where $\tau\equiv t$ and x ($\equiv r/\sigma_d\tau$) is the distance in a comoving frame. The continuity equation in the comoving frame then becomes

$$-x^2(2\alpha+x\frac{d\alpha}{dx})+\frac{d}{dx}(x^2v\alpha)=0. \tag{2}$$

This equation can be rewritten as $d(x^2(x-v)\alpha)/dx=x^2\alpha$. Comparing this equation with the relation between α and m, i.e., $dm/dx=x^2\alpha$, we find that the mass m can be expressed as $m(x)=x^2(x-v)\alpha$. This expression of $m(x)$ is substituted into the gravitational force to eliminate $m(x)$ in the momentum equation. Re-arrangement of the momentum equation

$$(v-x)\frac{dv}{dx}=-\frac{1}{\alpha}\frac{d\alpha}{dx}-(x-v)\alpha, \tag{3}$$

and Eq. (2) yields

$$\left[(x-v)^2-1\right]\frac{dv}{dx}=\left[\alpha(x-v)-\frac{2}{x}\right](x-v), \tag{4}$$

$$\left[(x-v)^2-1\right]\frac{1}{\alpha}\frac{d\alpha}{dx}=\left[\alpha-\frac{2}{x}(x-v)\right](x-v). \tag{5}$$

Note that Eqs. (4) and (5) have been derived in the past for describing the inside-out collapse of a singular isothermal molecular cloud (Shu 1977). However, our boundary conditions are different from those for the molecular cloud, in that the hot cluster is fed from outside by the expanding cold dark matter, and inside, the collisionless matter lands onto the compact core at a vanishing speed so that the particles can be captured. By contrast, the collapsing molecular cloud is fed from outside by a static isothermal gas sphere; inside, the collapsing gas lands on the protostar violently with a Mach number much greater than unity, and it relies eventually on the radiative cooling for the infall matter to be captured by the prostar.

Eqs. (4) and (5) can be simplified when the dark matter is cold, by setting the pressure term on the right of Eq. (3) to zero. It yields

$$\frac{dv}{dx}=\alpha \tag{6}$$

$$(x-v)\frac{1}{\alpha}\frac{d\alpha}{dx}=\alpha-\frac{2}{x}(x-v). \tag{7}$$

These equations are valid for the background dark matter particles before falling within the cluster. Note that both Eqs. (4) and (5), and Eqs. (6) and (7) allow for the Hubble-flow solution of a flat universe where $\alpha=2/3$ and $v=2x/3$.

Finally, the most relevant regime consistent with the current observations corresponds to a final saturated and static configuration when the matter infall ended before the present. That is, most of the available dark matter particles have collapsed into the cluster. Under these circumstances, such a saturated system is completely determined by the static forces in Eq. (3):

$$\frac{1}{\alpha}\frac{d\alpha}{dx}=-\frac{m}{x^2}. \tag{8}$$

Here, we have kept the same dimensionless parameterization although the dark matter density and mass are now time-independent. The additional factor τ in this dimensionless parameterization should be interpreted as the duration of cluster formation.

2.2. Infall boundary conditions

Our inner boundary condition of Eqs. (4) and (5) is so chosen that a growing massive compact core is present. For the collapsed particles to settle into the compact core, we demand that the cluster bulk flow should have a vanishing infall speed at the core. Quantitative details as to how the matter falls into the compact core will be further elaborated below.

Far from the cluster, we demand the pressure-free dark matter solutions to obey Eqs. (6) and (7), and they must either asymptotically match to a vanishing-density background when $\Omega\ll 1$, or asymptotically match to the Hubble flow ($\alpha=2/3, v=2x/3$) when $\Omega=1$. These pressure-free, outer infall solutions are then matched to the interior subsonic cluster solutions of Eqs. (4) and (5) through a co-moving conduction front. Technically, we must adjust both the location and strength of the conduction front to determine a unique solution satisfying both inner and outer boundary conditions.

2.3. Solution in an open universe ($\Omega\ll 1$) or the ongoing infall case

The background density of Hubble flow in this regime assumes a value $\alpha\ll 2/3$, and our outer infall solution should asymptotically decrease to match this low-density background far from the cluster. Practically, this boundary condition demands the asymptotic outer infall solution to vanish at large distances.

We shall stress that the solution to the open-universe case can also represent the situation where the self-similar infall began only recently in a flat universe, in which case τ is redefined as $t-t_1$, with t_1 being the starting time of infall and τ much less than the cosmic age t. As will be shown in the following analysis, the conduction front has a density $\rho\sim 1/4\pi G\tau^2$, much greater than the background density, e.g., the critical density $\rho_c(=1/6\pi Gt^2)$. Therefore the outer cold infall solution should asymptotically match the vanishingly small background density at large distances. Such a boundary condition is exactly the

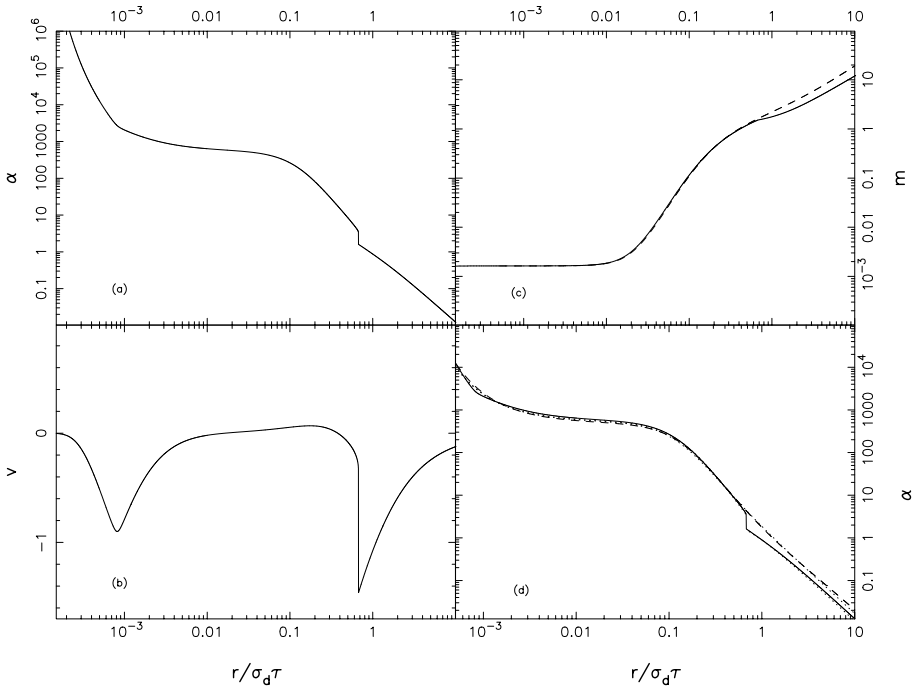

Fig. 1a – d. a Dimensionless density profile, **b** flow speed and **c** cluster mass obtained from the recent-infall, self-similar solutions under the initial and boundary conditions of a mass concentration $m_0 = 1.6 \times 10^{-3}$ within $x = r/\sigma_d\tau = 0.0005$. Also shown are the density **d** and mass **c** variations for a saturated cluster (dashed lines) expected under the same inner boundary condition. The dotted lines in **d** are the analytic fits of the density profiles by Eqs. (9) and (10), respectively.

same as the open-universe case. We shall briefly return to this case in Sect. 3.2 for a comparison with observations.

The outer pressure-free solution is constructed from a remote location far from the cluster by integrating Eqs. (6) and (7) inward. To ensure that the solution beyond the starting distance of integration indeed asymptotically matches onto the background flow, we perform an asymptotic analysis for the large-distance solution. The large-distance solution of Eqs. (6) and (7) is $\alpha = c_0/x^2$ and $v = -c_0/x$. That is, the density α and velocity v must be related in this specific way to warrant that the density asymptotically decreases to a sufficiently low value and matches onto the low background density. However, since Eqs. (6) and (7) are actually nonlinear equations, the amplitude c_0 must also be constrained in such a way that the outer infall solution be matched to the interior hot cluster solution through a conduction front. In this regard, the amplitude c_0 can be taken as a nonlinear eigenvalue imposed at the outer boundary. Moreover, the interior cluster solution is demanded to possess a diminishing velocity when the flow enters the compact core, so that the infall matter can be captured by the growing compact core. This requires a unique location for the conduction front as the second nonlinear eigenvalue.

To meet these non-trivial conditions, we find it useful technically to search for an approximate solution of Eqs. (4) and (5), which makes a smooth transition from a subsonic infall in the bulk to a supersonic infall into the core. This is because the trans-sonic solution is at the bifurcation boundary in the solution space (Shu 1977), and our desired solution is in the neighborhood of this boundary. The desired solution can then be constructed relatively easily after the approximate solution is found. Conditions for a flow to smoothly pass through the sonic speed are $\alpha_s = 2/x_s$ and $v_s = x_s - 1$, where the subscript s denotes the sonic point which is a critical point of Eqs. (4) and (5).

By adjusting both the amplitude c_0 of the asymptotic background solution and the location x_s of the sonic critical point, one may uniquely determine the location of and density jump at the conduction front, across which the mass flux and momentum flux in the co-moving frame are continuous. Our numerical search shows that the approximate solution has $c_0 \approx 1.22$ and $x_s \approx 10^{-3}$, and the location of the conduction front at $x_{cond} \approx 2/3$. Upstream of the conduction front, the dark matter density $\alpha \approx 1.6$ and infall speed $v \approx -1.45$, whereas downstream of the front, $\alpha \approx 3.5$ and $v \approx -0.32$. This conduction front has a moderate compression ratio ≈ 2.2.

An eigenvalue search in the neighborhood of this trans-sonic solution permits us to obtain the desired solution easily, which turns out to differ from the trans-sonic solution only near the compact core. As previously stated, the transonic solution is the bifurcating solution, and it has an infall speed increasing inward moderately. On one side of this bifurcation boundary, the infall speed increases drastically inward, but on the other side the infall speed turns around to become vanishingly small toward the core. (See Fig. 1.) (These situations are not unlike the behaviors of the scaling factor $a(t)$ in a flat universe, an open universe and a closed universe.) Clearly, the latter is what we look for. As the desired solution and trans-sonic solution are almost identical in most part of the cluster, their conditions at the conduction front are practically the same.

A caveat for our results is that the collisionless conduction front is likely to have a transition layer of finite thickness. Hence the results given above can only be regarded as a sophisticated estimate for modeling the boundary of the cluster, and the discontinuity obtained here should not be taken too literally.

The derived density profile of dark matter flow can be fit nicely by an analytical form:

$$\alpha(x) = \begin{cases} \frac{1.15}{(0.13^2+x^2)^{3/2}}\ e^{0.0015/x}; & 10^{-3} < x < x_{cond}; \\ \\ \frac{1.13}{0.52^2+x^2}; & 10 > x > x_{cond}. \end{cases} \quad (9)$$

Two separate components for the interior cluster solution are identified. The first component ($\propto e^{0.0015/x}$) gives rise to a peaked density profile, in response to the gravity of massive compact core; the second component represents the usual Bonner-Ebert state of isothermal sphere, which has a secondary core of size $x_c \approx 0.13$, and the density outside the outer core decreases outward first as x^{-3} and subsequently as x^{-2}. The conduction front is located roughly at the transition between the x^{-3} and x^{-2} profiles. The matter located in the region from $x \sim 0.02$ to $x \sim 0.4$ can be well approximated by a "static sphere", where the flow speed is roughly zero. Near the conduction front the infall speed sharply rises, and the finite flow speed immediately downstream of the conduction front serves only to flatten the density profile slightly. At about $x = 0.02$, the mass within this sphere is twice as much as that of the compact core; that is, the gravity arising from the massive compact core begins to be overwhelmed by the self-gravity of the matter outside the compact core. Figs. 1a, 1b and 1c depict the normalized density, velocity and mass profiles, respectively. Note that most part of the hot cluster is almost static, except near the conduction front and immediately outside the compact core.

2.4. Infall into the compact core

The compact core is a virialized bound object, where the density rises inwards more steeply than r^{-3}. As shown in Fig. 1 when the dark matter particles fall within $x = 0.02$, they experience solely the core gravity and are accelerated inward to reach a maximum speed at $x \sim 8 \times 10^{-4}$. Inside $x \sim 8 \times 10^{-4}$, the infall suddenly gets retarded by the core pressure and its speed decreases from this point on and becomes vanishingly small at the core center.

To pin down where the true core boundary is, we examine the binding energy. Inside the core, the flow must satisfy the binding condition, $|P.E.| \geq 2|K.E.|$, so that no particle may escape outside the radius x once enters. The specific potential energy $P.E.$ at the radius x is $-m/x$, and the specific kinetic energy $K.E.$ includes the specific thermal energy $3/2$ and the comoving flow energy $(v-x)^2/2$. Our solution shows that only inside $x = 5 \times 10^{-4}$ can the binding condition be satisfied. The size of the compact core is thus set to be $x_b = 5 \times 10^{-4}$.

2.5. Solution of early infall in a flat universe

The asymptotic solution far away from the cluster behaves as $v = (2x/3) - c_1/x$ and $\alpha = (2/3) + c_1/x^2$, when the deviation from the Hubble flow is small. We may employ the technique used in the previous case to obtain the solution in this regime. Surprisingly, the trans-sonic solution yields a conduction front at almost the same location and with a comparable jump as those of the previous case. The nonlinear eigenvalue x_s for the trans-sonic solution is also the same. In addition, the nonlinear eigenvalue c_1 also assumes a value equal to $c_1 = 1.22$. As a result, we find that the desired solution interior of the cluster is nearly the same as that of the previous case. The outer cold infall solution is, however, different from that in Eq. (9); the following analytical expression is found to fit the outer cold infall solution:

$$\alpha(x) = \frac{0.91}{x^{3/2}} + \frac{2}{3}; \quad 10 > x > x_{cond}. \quad (10)$$

2.6. Saturated phase

Taking the typical dark-matter velocity dispersion, $\sigma_d \approx 1000$ km s^{-1}, and the typical size of an Abell cluster, 3 Mpc, it follows that the typical time scale for cluster growth is on the order of 10^9 years, a short time compared with the age of the universe. Moreover, no strong cosmic evolution for clusters since $z \sim 0.8$ has been detected by recent X-ray observations (Rosati, et al. 1988; Vikhlinin et al. 1998). It is, therefore, reasonable to assume that most clusters have reached saturated states by $z \approx 0.8$. The comparison of observations with the present model is to be made primarily for the saturated state, where the clusters are virialized.

Because the central compact core is strongly gravitationally bound, the core should remain intact in the saturated phase, and the core size and mass are frozen to their values immediately before the infall stopped. Note that the extra factor τ that makes Eq. (7) dimensionless can be interpreted as the cosmic age at which the infall ended for an early formed cluster. Therefore, we may conveniently choose the same values of compact core mass ($m = 1.6 \times 10^{-3}$) and size ($x_b = 5 \times 10^{-4}$) as those of the infall phase for the static cluster solution.

The integration of Eqs. (2) and (7) can be carried out from the compact core outward to a sufficiently large distance to obtain the static cluster solution. The solution construction is straightforward once the core size and mass are specified. The resulting density profile of dark matter is plotted in Fig. 1d and can also be fit by an analytical form:

$$\alpha(x) = 1.68\ e^{0.0015/x}\ \frac{\sqrt{0.53^2 + x^2}}{(0.12^2 + x^2)^{3/2}}. \quad (11)$$

The density near the core also behaves as $\propto e^{0.0015/x}$, and again has a secondary outer core $x_c = 0.12$, beyond which the dark matter decreases outward also from a $\propto x^{-3}$ profile to $\propto x^{-2}$ profile at large distances. The corresponding profiles are depicted in Fig. 1c and 1d.

To sum up, for the solutions of both ongoing-infall (open universe) and early-infall (flat universe) cases, the interior hot clusters are found to be almost identical. This result to some degree reinforces the assertion of Gott (1975) that the self-similar evolution of bound objects depends weakly on the deceleration parameter. In the saturated phase, we have assumed that the compact core is frozen to the configuration immediately before the infall ended, and obtained a saturated cluster configuration that departs only slightly from those of the infall phase.

We also find that the plausible value for the compact core radius approximately equals $x_b \approx 5 \times 10^{-4}$ and the core mass, 1.6×10^{-3}. Taking a typical cluster for which $x = 1$ corresponds roughly to 1 Mpc and a typical velocity dispersion ∼1000 km s^{-1}, we estimate $x_b \sim 0.5$ kpc and the compact core mass about $3 \times 10^{11} M_\odot$.

3. Comparison with observations

3.1. Rationale and strategy

In this section, the predicted dark-matter distribution in the galaxy cluster will be tested against the observed results of gravitational lensing, galaxy distribution, gas distribution and baryon fractions. The rationale behind such a comparison is that if the theoretical prediction can well approximate the true dark-matter distribution, a single gravitational potential given by the predicted dark-matter distribution ought to be able to produce consistent profiles for these different observations. Our strategy is therefore first to use the gravitational lensing data to calibrate the length scale and depth of the gravitational potential, which are related to the only two parameters, τ and σ_d, in the theoretical model. Once the potential is fixed by the lensing data, the baryons will be treated as test particles, which should be so distributed as to be in dynamical equilibrium with the potential.

However, the construction of galaxy and gas distribution also requires an additional knowledge of their "equations of state". For galaxies, we adopt the average profile of the observed galaxy velocity dispersion and for gases, a polytropic equation of state. Though it can be relatively easy to find the best galaxy and gas parameters for a theoretical model to compare well with the observations, we would like to go one step beyond, and to constrain the choice of these empirical parameters based on a physical principle. That is, we consider the dark matter particles, galaxies and gases to have already been grossly virialized, and they should share a common *averaged* velocity dispersion since they are all within a common gravitational potential. It is under this additional constraint that the comparisons will be made.

3.2. Dark matter distribution: Comparison with the gravitational lensing results

Gravitational lensing appears to be a powerful and unique tool at present for probing the total matter distribution of galaxy clusters. It provides the gravitating masses of clusters regardless of the matter compositions and dynamical states. So far, the strongly and weakly distorted images of background galaxies have been detected in about 50 clusters at intermediate redshifts ranging from $z \approx 0.1$ to $z \approx 0.8$. These clusters constitute a good sample of matter distributions on scales $r \sim 10$ kpc – ~ 1 Mpc, both individually and statistically for testing various mass density profiles advocated by theoretical and observational studies. A direct comparison between our solution Eq. (11) and the gravitational lensing results is straightforward, provided that the evolutionary time τ and the velocity dispersion σ_d of dark matter particles are known. On the other hand, such a comparison will allow us to fix these two free parameters, if the self-similar solution predicts a consistent mass profile with what is derived from the gravitational lensing. Due to the cosmic variance, these two parameters can only be fixed sensibly by the averaged mass profile of the lensing results.

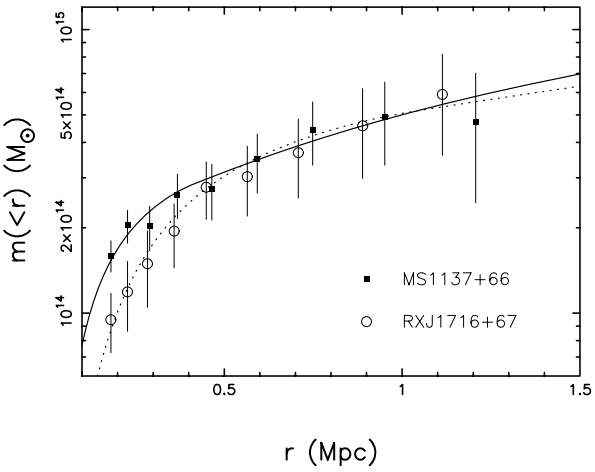

Fig. 2. A comparison between the projected cluster masses derived from the weakly distorted images of background galaxies behind clusters MS1137+66 and RXJ1716+67 and those from our saturation model. Data sets of the lensing cluster masses are from Clowe et al. (1998). Our best fitting yields $(\sigma_d, \sigma_d\tau) = (850$ km s^{-1},1.5 Mpc) and $(\sigma_d, \sigma_d\tau) = (1000$ km s^{-1},0.6 Mpc) for MS1137+66 and RXJ1716+67, respectively.

Before we fix these parameters by the averaged lensing results, a comparison with two individual clusters is presented to illustrate how well the theoretical profile may agree with the observed profiles individually, and not just statistically. Fig. 2 shows the projected radial mass distributions of two distant clusters at $z \approx 0.8$, MS1137+66 and RXJ1716+67, obtained recently by employing the mass reconstruction technique for the detected weak distortions of distant background galaxies (Clowe et al. 1998). Also plotted are the 2-D mass profiles from Eq. (11) for (σ_d, $\sigma_d\tau$)=(850 km s^{-1}, 1.5 Mpc) and (σ_d, $\sigma_d\tau$)=(1000 km s^{-1}, 0.6 Mpc), respectively. (From now on, the quantity τ should, unless otherwise indicated, be interpreted as the cluster formation time scale.) It appears that the self-similar solution does yield an acceptable fit to the results of MS1137+66 and RXJ1716+67. Moreover, the required values of velocity dispersion, $\sigma_d \sim 1000$ km s^{-1}, for dark matter are also in good agreement with the observed X-ray luminosity of the two clusters, $L_x \approx (6-8) \times 10^{44}$ erg s^{-1} in the energy band 0.3–3.5 keV. Meanwhile, the scale length $\sigma_d\tau \sim 1$ Mpc indicates a comfortable cluster formation time of $\tau \sim 10^9$ yrs.

This apparent success encourages us to conduct a comparison between the overall radial mass distribution of clusters revealed by the strong/weak lensing and that predicted by our analytical solutions. Note that in most cases, only the rich and X-ray luminous clusters of galaxies at intermediate redshifts are capable of gravitationally distorting the background galaxies. Namely, the (strong) lensing clusters alone are a fair sample of massive clusters at $\overline{z} \approx 0.3$ in the universe. We display in Fig. 3 the mean projected cluster mass m_{lens} within r, derived

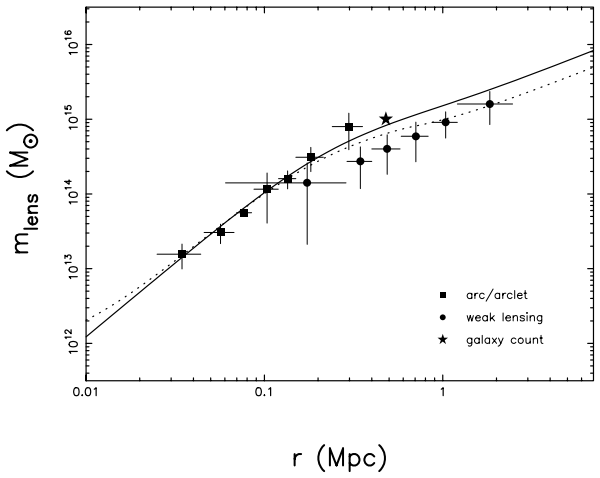

Fig. 3. An overall radial variation of the projected cluster masses revealed by the gravitational lensing methods: the strongly (arcs/arclets) and weakly distorted images of background galaxies (for references see Wu et al. 1998) as well as the deficit of red galaxies behind A1689 (Taylor et al. 1998). The results predicted by the recent-infall solution (dotted line) and the saturated configuration (solid line) are shown for $\sigma_d = 1300$ km s^{-1} and $\sigma_d\tau = 1$ Mpc.

from a total of 49 arcs/arclets in 38 clusters and 134 weak lensing measurements made among 24 clusters (Wu et al. 1998 and reference therein), in which we have not included the result of A2163. While there may exist a discrepancy between the strong and weak lensing measured cluster masses, the cluster masses obtained from three different lensing phenomena, including the deficit of red galaxy population detected behind A1689 due to the lensing magnification (Taylor et al. 1998), are essentially consistent within 2σ error bars. The radial mass variation of the lensing clusters from our self-similar solution with $\sigma_d = 1300$ km s^{-1} and $\sigma_d\tau = 1$ Mpc is also demonstrated in Fig. 3. The good fitness of our prediction to the lensing result is clearly seen. Since the velocity dispersions of optical galaxies in lensing clusters are in the range of 600 – 2000 km $^{-1}$ with an average value of 1200 km s^{-1} (Wu et al. 1998), the required mean velocity dispersion of dark matter particles $\sigma_d = 1300$ km s^{-1} is more than acceptable. Consequently, the mean formation time of the lensing and massive clusters turns out to be $\tau = 7.5 \times 10^8$ yrs. This timescale seems to be relatively short though it is not impossible for the very rich clusters (Gunn & Gott 1972).

With the same velocity dispersion and scale length parameters, our theoretical results produce equally good fits for the mass profiles given by both the static solution of Eq. (11) and the collapsing solution of Eq. (9). The latter should now be interpreted as the solution of a growing cluster which began its formation only recently. Also shown in Fig. 3 is that the difference between the mass profiles is only minor, leading to an inability to observationally distinguish the two models simply from their mass profiles. To differentiate these two models, it is helpful to recall some established observational evidences of galaxy clusters. It was shown more than a decade ago that optical counts of clusters did not exhibit any evolutionary tendencies for redshift out to at least $z \approx 0.5$ (Gunn, Hoessel, & Oke 1986). The same conclusion holds true for the X-ray selected clusters since redshift of as high as $z \sim 0.8$ (Rosati et al. 1998 and references therein). Furthermore, no significant differences in the dynamical properties between low-redshift and high-redshift clusters, such as the X-ray luminosity-temperature relationship, the velocity dispersion-temperature relationship (Mushotzky & Scharf 1997; Wu et al. 1999), and the baryon fraction (see Fig. 7), have been detected. In particular, the distribution of core radii of the intracluster gas in nearby clusters is identical to that of distant clusters ($z > 0.4$) (Vikhlinin et al. 1998). This last point can be regarded as the most convincing evidence for the already "settled" configuration of cluster matters, but sharply discords with an evolving self-similar model, which predicts the core radius to be much smaller in the past (Kaiser 1986). Suggested by these evidences can be that significant matter infall processes should have already ended before $z \sim 0.4$ so that the global properties of galaxy clusters have remained approximately unchanged since an even earlier epoch.

3.3. Galaxy distribution

The rationale of the following exercise goes as follows. From the massive-cluster samples measured by gravitational lensing, we have statistically determined the mean velocity dispersion $\sigma_d (\approx 1300$ km s$^{-1})$ and the mean length scale $\sigma_d\tau$ (≈ 1 Mpc), thereby fixed the average mass and length scales of our solutions for massive clusters. This predicted average solution hence has *no* adjustable parameter. So, we may employ the Jeans equation to construct an expected average galaxy distribution and compare it with the observed average galaxy distribution within the massive clusters.

So far we have not yet included the baryonic matter (galaxies and gas) in our self-similar solutions of dark matter particles in clusters. Although an exact self-similar solution with a proper combination of the collisionless dark matter and the collisional gas infall can be constructed, we would rather take a less vigorous approach to this problem by treating the baryons as test particles. For galaxy populations characterized by their radial velocity dispersion $\sigma_{gal}(r)$ and number density $n_{gal}(r)$, the Jeans equation under the light-traces-mass hypothesis reads

$$\frac{1}{n_{gal}}\frac{d(\sigma_{gal}^2 n_{gal})}{dr} + \frac{2\sigma_{gal}^2}{r}A = -\frac{GM}{r^2}, \tag{12}$$

where M is the total cluster mass (we use dark matter instead) enclosed within radius r, and A denotes the velocity anisotropy parameter. Since the above equation corresponds to a purely hydrostatic equilibrium, we employ the static solution, Eq. (11), to evaluate $M(r)$. (The collapsing solution, Eq. (9), has also been tested, and essentially the same $M(r)$ is obtained.) Once the velocity profile $\sigma_{gal}(r)$ and A are specified, we can easily work out the galaxy number density profile according to Eq. (12).

We compare our prediction with the average surface number density of galaxies over 14 distant clusters measured by the Canadian Network for Observational Cosmology (CNOC) (Carlberg, Yee, & Ellingson 1997). Actually, the majority of the 14 clusters are those massive lensing clusters discussed in the

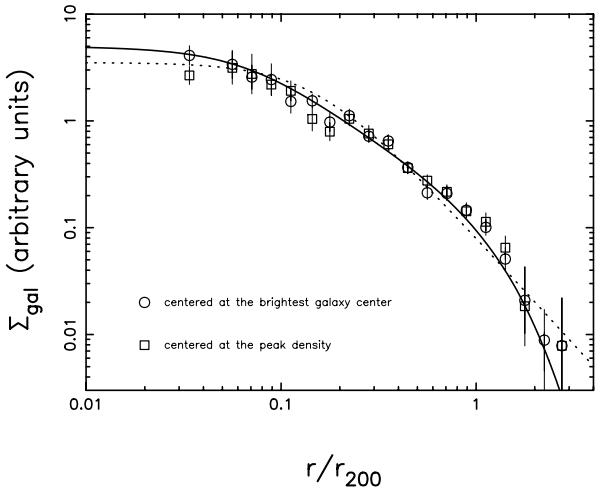

Fig. 4. Surface number density profile of galaxies over an ensemble of 14 distant clusters from CNOC (Carlberg, Yee, & Ellingson 1997). Solid line is our expected result of the saturation model for $\sigma_d/\sigma_{gal}(0) = 0.78$ and $r_{200}/\sigma_d\tau = 0.4$ under the assumption that galaxies trace the gravitational potential of dark matter particles in clusters. The conventional King model fit is illustrated by the dotted line.

above subsection. We adopt the simple form of the radial velocity dispersion suggested by CNOC, $\sigma^2_{gal}(r) = \sigma^2_{gal}(0)/(1 + r/r_{200})$ and the assumption for a zero anisotropy parameter, $A = 0$. Here, $\sigma_{gal}(0)$ is the central velocity dispersion and r_{200} denotes the radius within which the mean cluster mass density is 200 times the critical mass density of the universe ($\Omega_0 = 1$). The mean value of r_{200} over the 14 CNOC clusters has been found to be $r_{200} = 2.5$ Mpc.

With the predicted gravitational potential of the underlying dark matter and the given profile of observed velocity dispersion of galaxies, one can solve for the average galaxy distribution using the Jeans equation, Eq. (12). In the following comparison, we will instead take an alternative route by first seeking the best fit parameters and then examine how well they may agree with those fixed by the lensing results. Fig. 4 shows the CNOC galaxy surface number density Σ_{gal} and the predicted galaxy surface number density from our model for the best fit $\sigma_d/\sigma_{gal}(0) = 0.78$ and $\sigma_d\tau/r_{200} = 0.4$. When combined with $r_{200} = 2.5$ Mpc, this choice of length scale $\sigma_d\tau (= 0.4 r_{200} = 1$ Mpc) is what has previously been determined by the gravitational lensing. The good fit of the predicted length scale with the observed length scale is remarkable.

The magnitude of the predicted surface number density depends sensitively on the central velocity bias $\sigma_d/\sigma_{gal}(0)$. Its best fit value being less than unity may simply reflect the fact that the central galaxy velocity $\sigma_{gal}(0)$ is higher than the average value $\overline{\sigma}_{gal}$. To pin down the ratio of the averaged specific kinetic energy of galaxies to that of dark matter particles for this value of $\sigma_{gal}(0)$, we calculate

$$\frac{\sigma_d^2}{\overline{\sigma}^2_{gal}} = \sigma_d^2 \Bigg/ \left(\frac{\int_{x_b}^{\infty} \sigma^2_{gal}(x)\Sigma_{gal}(x)xdx}{\int_{x_b}^{\infty} \Sigma_{gal}(x)xdx} \right) \tag{13}$$

A straightforward calculation shows that $\sigma_d/\overline{\sigma}_{gal} \approx 1$. That is, the best-fit central velocity bias $\sigma_d/\sigma_{gal}(0)$ renders the average specific kinetic energies of both dark matter particles and galaxies to be approximately equal, as required by our principle set forth to constrain the empirical parameters. The good agreement is more than surprising for such a simple theoretical model. Actually, it has already been seen in the above subsection that the velocity dispersion of dark matter particles ($\sigma_d = 1300$ km s^{-1}), required to account for the projected mass distribution of clusters derived from gravitational lensing, is roughly the same as the reported mean value for the CNOC galaxies ($\overline{\sigma}_{gal} = 1200$ km s^{-1})). This is also in agreement with the previous results given by a statistical comparison of cluster mass determinations from gravitational lensing and velocity dispersion of cluster galaxies as the tracer of cluster potential (Wu & Fang 1997; Wu et al. 1998).

3.4. Gas distribution and β model

Similarly, the equation of hydrostatic equilibrium can also be applicable to the hot X-ray emitting gas of number density $n_{gas}(r)$ in clusters (Cavaliere & Fusco-Femiano 1976):

$$\frac{1}{n_{gas}} \frac{d(\sigma^2_{gas} n_{gas})}{dr} = -\frac{GM}{r^2}, \tag{14}$$

in which $\sigma^2_{gas} \equiv kT/\mu m_p$ is the "equivalent velocity dispersion" of gas with μm_p being the mean particle mass. Assuming an equation of state for the gas $T = T_0[n_{gas}/n_{gas}(0)]^{\gamma-1}$, we can write out the gas number density profile in terms of Eq. (14):

$$\frac{n_{gas}}{n_{gas}(0)} = \left[1 - \frac{\gamma - 1}{\gamma} \int_{r_b}^{r} \frac{GM}{\sigma^2_{gas}(0) r^2} dr \right]^{1/(\gamma-1)}, \tag{15}$$

where r_b is the physical length corresponding to x_b. Motivated by the fact that $\overline{\sigma}_{gal} \approx \sigma_d$, the arbitrariness of the polytropic index γ and $\sigma_{gas}(0)$ can be fixed by a physical requirement that $\overline{\sigma}_{gas}$ also equals σ_d, where $\overline{\sigma}_{gas}$ is the average equivalent velocity dispersion of gas:

$$\overline{\sigma}^2_{gas} = \frac{\int_{x_b}^{\infty} \sigma^2_{gas}(x) S(x) x dx}{\int_{x_b}^{\infty} S(x) x dx}. \tag{16}$$

The observed X-ray surface brightness is related to the temperature and number density of electrons in clusters as

$$S_x(r) \propto \int_r^{\infty} T^{1/2}(x) n^2_{gas}(x) \frac{x dx}{\sqrt{x^2 - r^2}}, \tag{17}$$

provided that the radiation mechanism is the thermal Bremsstrahlung with a Gaunt factor weakly dependent on T.

Before proceeding to a discussion on the general properties of the theoretically predicted X-ray surface brightness profile, we first present a comparison of the predicted profile with the observed X-ray surface brightness of an individual cluster for an illustration of the agreement that also holds individually. Fig. 5 shows a typical example of the *ROSAT* observed $S_x(r)$ for cluster Cl0016+16 ($z = 0.55$), together with our expected $S_x(x)$

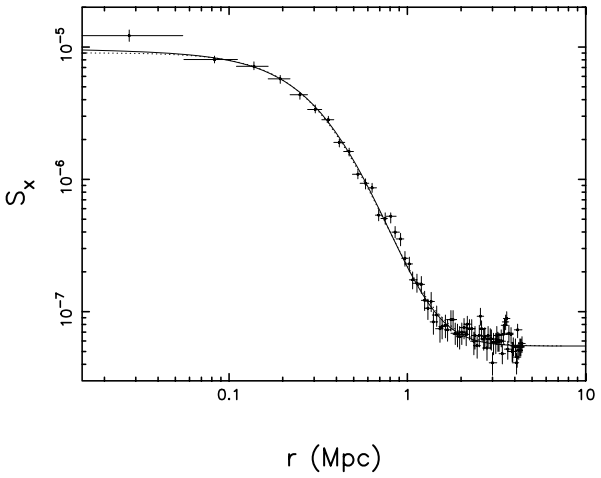

Fig. 5. An examples of fit of the theoretically predicted X-ray surface brightness (solid lines) to the observation of Cl0016+16 (Neumann & Böhringer 1997). The best β model fit is also displayed (dotted lines) for comparison. A background surface brightness of 5.5×10^{-8} s^{-1} arcsec^{-2} is assumed.

from Eqs. (15) and (17). The latter are obtained by properly choosing the length scale parameter $\sigma_d\tau$ and the central biasing parameter $\sigma_d/\sigma_{gas}(0)$ or equivalently the polytropic index γ. This procedure is somewhat equivalent to the conventional β model fit by properly determining the X-ray core radius and the power index. Yet, unlike the β model which is purely an empirical formula, our predicted X-ray surface brightness profile is given by the hydrostatic equilibrium of the intracluster gas with the underlying gravitational potential of the cluster dark matter particles. The physics behind our prediction about the gas distribution is well understood.

Fig. 6 shows the X-ray surface brightness profiles of clusters obtained from Eqs. (15) and (17) for a set of polytropic indices γ =1.05, 1.1, 1.2 and 1.3, in which we have imposed a constraint on $\sigma_d/\sigma_{gas}(0)$ by requiring $\sigma_d/\overline{\sigma}_{gas} = 1$, which uniquely defines a central biasing parameter $\sigma_d/\sigma_{gas}(0)$ for each value of γ. We now superpose the conventional β models on the theoretically expected S_x. Surprisingly, all the derived S_x profiles can be well approximated by the β models except near the compact cores, where brightness cusps may appear in some cases. The allowed β parameters are dependent on the adopted γ, with a smaller β for a large γ. Additionally, our fitted β parameters are consistent with the observed β parameters in the range of $\beta_{fit} \sim 0.6 - 1.2$. If the average value of β_{fit} is indeed around $2/3$ as indicated by most current observations, we may conclude that a large proportion of galaxy clusters should have a mean polytropic index of $\gamma \approx 1.2$–1.3. This point has recently been verified by the X-ray measurements of temperature structures of 30 nearby clusters (Markevitch et al. 1998), all of which show similar temperature profiles with a polytropic index of $\gamma = 1.2$–1.3.

On the other hand, the above fits for various γ's yield that the core radius of the gas profile varies from $r_c/\sigma_d\tau \sim 0.16$ to ~ 0.30. Of these, the choice for $\gamma = 1.2$ that yields $r_c/\sigma_d\tau \approx 0.20$ is again of particular interest. Since if the mean length scale $\sigma_d\tau$ is approximately ~ 1 Mpc for rich clusters, as was shown in the above two subsections, this choice implies a mean core radius of $r_c \approx 0.2$ Mpc in S_x; this core radius is comparable to the median values (0.21–0.24 Mpc) of the X-ray core radius distributions of the *ROSAT* detected clusters (Vikhlinin et al. 1998). Taking these results as a whole, we have provided a consistent scenario for the physical origin of the conventional β model.

To sum up, our fit suggests that the gas components of clusters have an overall polytropic index close to $\gamma \approx 1.2$ and a mean β parameter $\overline{\beta}_{fit} \approx 2/3$. It is worth stressing again that by requiring the ratio of mean specific kinetic energy in galaxy to that in gas to be unity, $\beta_{spec} \equiv \overline{\sigma}^2_{gal}/(k\overline{T}_{gas}/\mu m_p) = \overline{\sigma}^2_{gal}/\overline{\sigma}^2_{gas} = (\sigma_d/\overline{\sigma}_{gas})^2/(\sigma_d/\overline{\sigma}_{gal})^2 \approx 1$, the two β values, $\overline{\beta}_{fit}$ and β_{spec}, turn out to agree nicely with the observationally determined ones (Wu, Fang & Xu 1998). The two β's are not the same, and the so-called "β discrepancy" (Bahcall & Lubin 1994; references therein) appears to be a natural consequence of our model. We have also noticed that a similar effort was recently made by Makino, Sasaki & Suto (1998) based on the universal dark matter profile. However, while their derived X-ray surface brightness is well represented by the β model in shape, their predicted core radius is a factor of (3–10) smaller than the actually observed values.

3.5. Baryon fraction

Having known the dark matter and gas distributions, we can easily provide the baryon (gas) fractions of clusters $f_b \equiv M_{gas}(r)/M_{total}(r)$, where M_{gas} and M_{total} are the gas and total masses enclosed within the radius r, respectively. Of course, the absolute value of f_b is ultimately related to the amplitude of gas density profile, $n_{gas}(0)$, which has remained unknown thus far. Although we shall be able to figure out $n_{gas}(0)$ using the observationally determined baryon fractions, a particular attention is paid to the issue of how the baryon fractions vary with scales. Fig. 7 demonstrates the cluster baryon fractions versus radii obtained through the deprojection analysis of *Einstein Observatory* data for 207 clusters (White, Jones & Forman 1997). Basically, the baryon fraction is an increasing function with radius and tends towards an asymptotic value of $\sim 20\%$–30% at large radius. Such a variation has been noticed previously by a number of authors (e.g. White & Fabian 1995; David 1997; White et al. 1997) but not yet been satisfactorily accounted for in the framework of any prevailing models for cluster formation.

Adopting a mean polytropic index of $\gamma = 1.2$ for the X-ray gas, we attempt to reproduce the observed radial variation of baryon fractions with our model. Since the length scale of our model has already been fixed, the fitting can only be conducted in terms of the absolute value of baryon fractions. The best-fit curve to is illustrated in Fig. 7. The significant rise of f_b with radius from $r \sim 0.1$ Mpc outward is due to the fact that in this radial interval the dark matter profile goes as r^{-3} (Fig. 1) whereas the gas distribution varies as r^{-2} (Fig. 6c). However, it should be pointed out that the validity of our prediction about f_b outside $r \sim 5$ Mpc begins to be questionable, though a decreasing tendency is seen to occur beyond $r \sim 10$ Mpc.

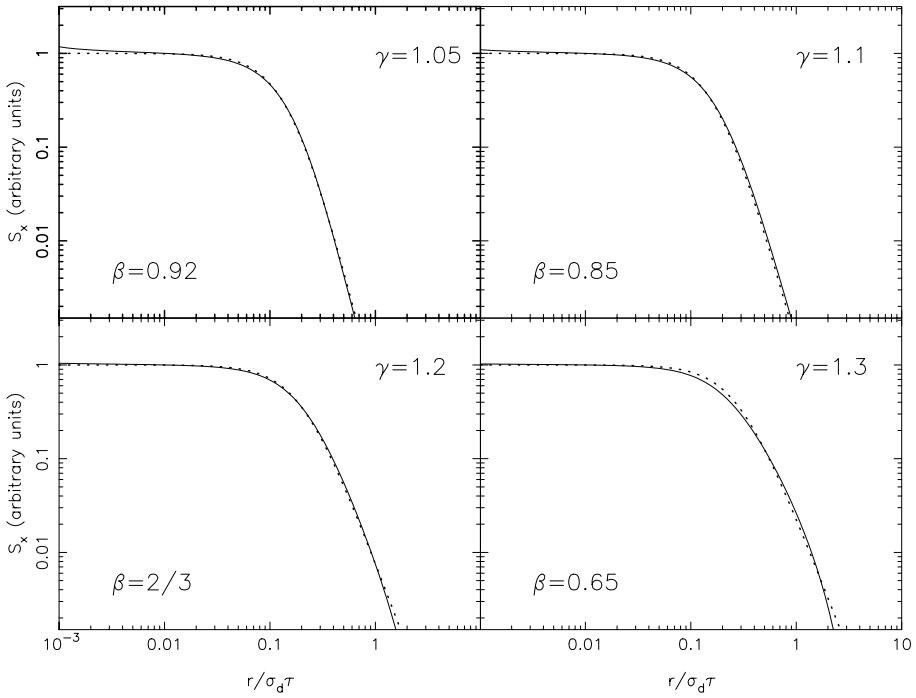

Fig. 6a – d. X-ray surface brightness profiles predicted for different polytropic indices $\gamma = 1.05$ (a), 1.1 (b), 1.2 (c) and 1.3 (d) in the equation of state $T \propto n^{\gamma-1}$ (solid lines). The requirement that the mean kinetic energy of dark matter particles is equal to that of gas, $\sigma_d^2 = (k\overline{T}/\mu m_p)$ has been employed. Also plotted are the conventional β gas profiles (dotted lines).

Finally, we have noted that the majority of the data for the baryon fractions f_b have so far been derived from the isothermal gas hypothesis, for which an emission-weighted temperature over a finite X-ray emitting surface is applied. Therefore, the comparison between our prediction with the measured baryon fractions holds true only statistically.

4. Discussions and conclusions

In the present work, we explore the possibility of building up two distinct mass cores in a single galaxy cluster as a result of matter infall from the background Hubble flow. Comparisons of the predicted saturated configuration with observations reveal that our model agrees quite well with the lensing, galaxy distribution and gas distribution. Our result is insensitive to the density parameter Ω since the cluster builds up within a period much shorter than the age of the universe. The key assumptions of this model are (a) a pre-existing mass concentration, onto which the background matter falls, (b) the infall within the cluster is subsonic and the dark matter particles are largely virialized with ergodic orbits, in which situation the particle velocity dispersion is assumed to be a constant and (c) in the saturated phase the mass ratio of the two cores remains the same as that in the infall phase.

Despite of its oversimplification, the self-similar gravitational collapse of collisionless dark matter particles remains to be the only analytic approach to access the dynamical process of cluster formation, which may complement our understanding of its physical causes in addition to the employment of large-scale numerical simulations. In this paper we have re-addressed the self-similar infall model in a new way: Our initial and boundary conditions are so chosen that there is a pre-existent mass concentration in the central position of cluster to induce mass accretion, and the process of major dark matter infall is confined within a finite interval of $\sim 10^9$ years. Consequently, a hydrostatic equilibrium is established by now between the gravitational potential of dark matter and the galaxies/gas in the late evolutionary stage of clusters (probably since redshift $z \sim 0.8$). In the scenario that the global properties of clusters remain not evolving, we have successfully reproduced the distributions of

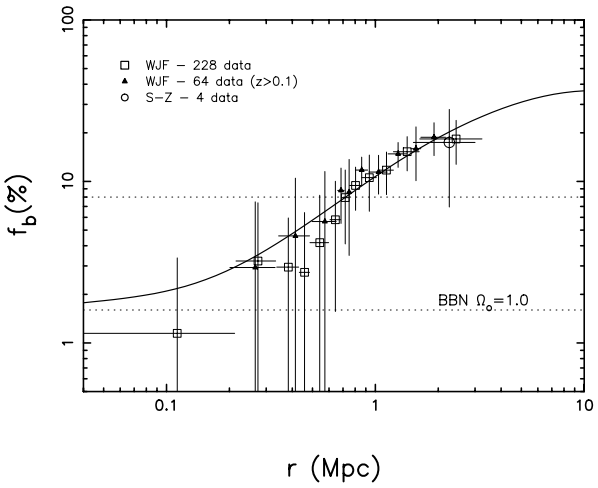

Fig. 7. The binned radial variation of baryon (gas) fractions (f_b) of clusters. The data sets are from the *Einstein Observatory* (White, Jones, & Forman 1997; WJF) and from the measurements of the S-Z effects in four clusters (Myers et al. 1997). The high-redshift clusters ($z > 0.1$) in WJF are explicitly plotted for comparison. The allowed cosmological baryon fraction in the standard Big Bang Nucleosynthesis (BBN) for a matter dominant flat universe is also illustrated. The solid line is the theoretically predicted baryon fraction by our saturation model for gas with $\gamma = 1.2$ and $\sigma_d/\sigma_{gas}(0) = 0.62$

total mass, galaxies and hot gas in clusters of galaxies revealed by gravitational lensing and optical/X-ray observations. Apart from the very central massive core of $\sim$ few $10^{11} M_\odot$ within the radius of ~ 1 kpc (adopting $\sigma_d = 10^3$ km s^{-1} and $\sigma_d \tau = 1$ Mpc), the dark matter, galaxies and gas essentially share a common "secondary" core at $r \sim 0.15 - 0.2$ Mpc, though their profiles can differ significantly, depending on the radial variations of the velocity dispersion/thermal speed of galaxies/gas.

We also find that the bias of the cluster averaged velocity dispersion of galaxies against the velocity dispersion of dark matter is indeed approximately unity, i.e., $\overline{\sigma}_{gal}/\sigma_d \approx 1$, as expected from the virialization consideration that they are both within the same gravitational potential. In view of this result, it is further demanded that the specific dark matter kinetic energy and specific gas thermal energy to also be equal, i.e., $(k\overline{T}_{gas}/\mu m_p)/\sigma_d^2 \approx 1$, thus yielding the β_{spec} parameter, which denotes the ratio of specific kinetic energy in galaxy to that in gas, to be also approximately unity (Bahcall & Lubin 1994; Girardi et al. 1996). The resulting X-ray surface brightness is found to be well fit by the conventional β-model, with, however, the parameter β_{spec} different from the β_{fit} parameter used in the β-model fitting of the X-ray surface brightness. The mean value of β_{fit} turns out to be $\overline{\beta}_{fit} \approx 2/3$, in contrast to $\beta_{spec} \approx 1$. Therefore, the β discrepancy, $\beta_{spec}/\beta_{fit} \neq 1$, arises, in our model, as a natural consequence of the polytropic index of gas $\gamma \neq 1$. With the mean value $\overline{\beta}_{fit} \approx 2/3$, it yields that the mean value of γ should be $\gamma \approx 1.2$.

Apparently, the present model has its own problems that remain to be resolved in the future. First of all, it is unclear at what epoch the central massive core should begin to form; this issue is relevant to the question as to when our model starts to be applicable. Second, although optical/X-ray observations prefer a non-evolutionary scenario of galaxy clusters within $z \sim 0.8$, we are unaware of how the background matters should terminate the infall onto clusters. It is possible that after the cluster mass reached some threshold value the intercluster matters could then be heated up by the intracluster tidal forces exerted by clusters, thereby preventing further matter infall. How this heating mechanism may proceed remains to be examined. Finally, the massive compact core is predicted to be about 1 kpc in size. However, the current observations are unable to set any robust constraints on the matter distribution inside the core region as small as $r < 10$ kpc. It requires future observations to confirm our prediction of compact cores at the cluster centers.

Acknowledgements. We gratefully acknowledge the insightful comments by an anonymous referee. This work was supported by the National Science Council of Taiwan, under Grant No. NSC87-2816-M008-010L and NSC87-2112-M008-009, and the National Science Foundation of China, under Grant No. 19725311.

References

Bahcall N.A., Lubin L.M., 1994, ApJ 426, 513
Bertschinger E., 1985, ApJS 58, 39
Binney J., Tremaine S., 1987, Galactic Dynamics. Princeton Univ. Press, Princeton, p. 308
Carlberg R.G., Yee H.K.C., Ellingson E., 1997, ApJ 478, 462
Cavaliere A., Fusco-Femiano R., 1976, A&A 49, 137
Clowe D., Luppino G.A., Kaiser N., Henry J. P., Gioia I.M., 1998, ApJ 497, L61
Cole S., Lacey C., 1996, MNRAS 281, 716
David L.P., 1997, ApJ 484, L11
Durret F., Gerbal D., Lachièze-Rey M., Lima-Neto G., Sadat R., 1994, A&A 287, 733
Eke V.R., Navarro J.F., Frenk C.S., 1998, ApJ 503, 569
Fan X., Bahcall N.A., Cen R., 1997, ApJ 485, L53
Fillmore J.A., Goldreich P., 1984, ApJ 281, 1
Fukushige T., Makino J., 1997, ApJ 477, L9
Girardi M., Fadda D., Giuricin G., Mardirossian F., Mezzetti M., 1996, ApJ 457, 61
Giraud E., 1999, ApJ 512, 25
Gott J.R. III, 1975, ApJ 201, 296
Grossman S.A., Saha P., 1994, ApJ 431, 74
Gunn J.E., Hoessel J.G., Oke J.B., 1986, ApJ 306, 30
Gunn J.E., Gott J.R. III, 1972, ApJ 176, 1
Hammer F., 1991, ApJ 383, 66
Kaiser N., 1986, MNRAS 222, 323
Kaiser N., 1991, ApJ 383, 104
Lynden-Bell D., 1967, MNRAS 136, 101
Makino N., Sasaki S., Suto Y., 1998, ApJ 497, 555
Markevitch M., Forman W.R., Sarazin C.L., Vikhlinin A., 1998, ApJ 503, 77
Merritt D., Tremaine S., Johnstone D., 1989, MNRAS 236, 829
Mushotzky R.F., Scharf C.A., 1997, ApJ 482, L13
Myers S.T., Baker J.E., Readhead A.C.S., Leitch E.M., Herbig T., 1997, ApJ 485, 1
Navarro J.F., Frenk C.S., White S.D.M., 1995, MNRAS 275, 720
Navarro J.F., Frenk C.S., White S.D.M., 1997, ApJ 490, 493
Neumann D.M., Böhringer H., 1997, MNRAS 289, 123
Press W.H., Schechter P., 1974, ApJ 187, 425
Rosati P., Ceca R.D., Norman C., Giacconi R., 1998, ApJ 492, L21
Shu F.H., 1977, ApJ 214, 488
Taylor A.N., Dye S., Broadhurst T.J., Benitez N., van Kampen E., 1998, ApJ 501, 539
Teyssier R., Chièze J.-P., Alimi J.-M., 1997, ApJ 480, 36
Vikhlinin A., McNamara B.R., Forman W., et al., 1998, ApJ 498, L21
White D.A., Fabian A.C., 1995, MNRAS 273, 72
White D.A., Jones C., Forman W., 1997, MNRAS 292, 419
Williams L.L.R., Navarro J.F., Bartelmann M., 1999, ApJ, submitted (astro-ph/9905134)
Wu X.-P., Chiueh T., Fang L.-Z., Xue Y.-J., 1998, MNRAS 301, 861
Wu X.-P., Hammer F., 1993, MNRAS 262, 187
Wu X.-P., Fang L.-Z., 1997, ApJ 483, 62
Wu X.-P., Fang L.-Z., Xu W., 1998, A&A 338, 813
Wu X.-P., Xue Y.-J., Fang L.-Z., 1999, ApJ 524, 22